Seasonal variation of ozone and black carbon observed at Paknajol, an urban site in the Kathmandu Valley, Nepal

D. Putero[1], P. Cristofanelli[1], A. Marinoni[1], B. Adhikary[2], R. Duchi[1], S. D. Shrestha[3], G. P. Verza[4], T. C. Landi[1], F. Calzolari[1], M. Busetto[1], G. Agrillo[1], F. Biancofiore[5], P. Di Carlo[5], A. K. Panday[2], M. Rupakheti[6], and P. Bonasoni[1]

[1] {CNR-ISAC, National Research Council of Italy - Institute of Atmospheric Sciences and Climate, Via Gobetti 101, 40129, Bologna, Italy}
[2] {ICIMOD, International Centre for Integrated Mountain Development, G.P.O. Box 3226, Khumaltar, Lalitpur, Kathmandu, Nepal}
[3] {Ev-K2-CNR Committee, G.P.O Box 5109, Paknajol, Kathmandu, Nepal}
[4] {Ev-K2-CNR Committee, Via S. Bernardino 145, 24126, Bergamo, Italy}
[5] {Center of Excellence CETEMPS, University of L'Aquila, Via Vetoio 1, 67010, Coppito (AQ), Italy}
[6] {IASS, Institute for Advanced Sustainability Studies, Berliner Strasse 130, 14467, Potsdam, Germany}

Correspondence to: D. Putero (d.putero@isac.cnr.it)

Abstract

The Kathmandu Valley in South Asia is considered as one of the global "hot spots" in terms of urban air pollution. It is facing severe air quality problems as a result of rapid urbanization and land use change, socioeconomic transformation and high population growth. In this paper, we present the first full year (February 2013 – January 2014) analysis of simultaneous measurements of two short-lived climate forcers/pollutants (SLCF/P), i.e. ozone (O_3) and equivalent black carbon (hereinafter noted as BC) and aerosol number concentration at Paknajol, in the center of the Kathmandu metropolitan city. The diurnal behavior of equivalent black carbon (BC) and aerosol number concentration indicated that local pollution sources represent the major contributions to air pollution in this city. In addition to photochemistry, the planetary boundary layer (PBL) and wind play important roles in determining O_3 variability, as suggested by the analysis of seasonal changes of the diurnal cycles and the correlation with meteorological parameters and aerosol properties. Especially during pre-monsoon, high values of O_3 were found during the afternoon/evening. This could be related to mixing and entrainment processes between upper residual layers and the PBL. The high O_3 concentrations, in particular during pre-monsoon, appeared well related to the impact of major open vegetation fires occurring at regional scale. On a synoptic-scale perspective, westerly and regional atmospheric circulations appeared to be especially conducive for the occurrence of the high BC and O_3 values. The very high values of SLCF/P, detected during the whole measurement period, indicated persisting adverse air quality conditions, dangerous for the health of over 3 million residents of the Kathmandu Valley, and the environment. Consequently, all of this information may be useful for implementing control measures to mitigate the occurrence of acute pollution levels in the Kathmandu Valley and surrounding area.

1. Introduction

Air pollution is a major environmental challenge in several regions of the world, defined as "hot spots" (Monks et al., 2009). In South Asia, by using in situ measurements, chemical transport models and satellite observations, Ramanathan et al. (2007) identified layers of regional-scale plumes of atmospheric pollutants that extended from the Himalayas to the northern Indian Ocean, including high levels of short-lived climate forcers/pollutants (SLCF/P), such as black carbon (BC) and ozone (UNEP and WMO, 2011). Several significant implications of these compounds were recognized for the global climate (Ramanathan and Carmichael, 2008), regional climate and crop yields, and for human health (Shindell et al., 2012).

The Kathmandu Valley in Nepal, the largest metropolitan region at the Himalayan foothills (one of the most polluted but still least sampled regions of the world), represents one of the regional hot spots in terms of air pollution. This area, having a cross section of about 20 km north to south and 30 km east to west, comprises of three administrative districts, Kathmandu, Lalitpur and Bhaktapur, and has undergone rapid but unplanned urbanization due to high population growth, dramatic land use changes and socioeconomic transformation, thus facing severe air pollution problems. Over the past quarter century the Kathmandu Valley's population has quadrupled to more than 3 million. Between 1990 and 2014 the total vehicle fleet grew from 45,871 to more than 700,000, with the number of motorcycles having the highest annual growth rate of 16% during the period (Faiz et al., 2006; Shrestha et al., 2013). Furthermore, by using an energy system model, Shrestha and Rajbhandari (2010) indicated that the total energy consumption in the Kathmandu Valley is expected to increase at an average growth rate of 3.2% in the period ranging from 2005 to 2050. By 2050, there will be an increase in the energy consumption of 30%, 25% and 22% for the shares of transport, industrial and commercial sectors, respectively. In the Kathmandu city center the air quality is so bad that Nepal's own national ambient air quality standards are only met on about 40 days per year; during the rest of the period the particulate matter exceeds the limit considered harmful. The Kathmandu Valley sizable emission of air pollutants is of concern for local and regional air quality and climate; however, it is still a manageable size in terms of potential interventions to address serious air pollution problems in the valley. The relative importance of local and regional emission sources has not been well quantified yet, making it difficult to design mitigation strategies that will have a large impact and still be cost-effective. Therefore, an improved scientific understanding of the main sources and impacts of air pollution in the region is a prerequisite for designing effective mitigation options.

In the recent past, several studies have presented measurements of various atmospheric compounds in the Kathmandu Valley (e.g. Sharma et al., 2012; Panday and Prinn, 2009; Panday et

al., 2009; Pudasainee et al., 2006; Giri et al., 2006; Sharma et al., 1997; Shrestha and Malla, 1996), all suggesting that air pollution in Kathmandu has harmful effects on human health (leading to bronchitis, throat and chest diseases), crop productivity and also tourism income in Nepal, being Kathmandu the heart of the Nepalese culture, art and architecture. However, none of them presented simultaneous observations of key SLCF/P across seasons.

In order to provide continuous measurements of atmospheric composition variability, a measurement site was installed in 2013 at Paknajol, in the tourist area of the Kathmandu city. This has enabled us to achieve a more comprehensive understanding of the dynamics of air pollution and related emissions in the Kathmandu Valley, and to constitute the scientific basis in order to support the local implementation of mitigation actions. These measurements were carried out as part of the SusKat-ABC (A Sustainable Atmosphere for the Kathmandu Valley – Atmospheric Brown Cloud) campaign in Nepal, the second largest international air pollution measurement campaign ever carried out in southern Asia, which aim is to provide the most detailed air pollution measurements to date for the Kathmandu Valley and the surrounding region (Rupakheti et al., 2015).

2. Materials and Methods

2.1 Measurement site and instrumental setup

Kathmandu city is located in a broad basin at the foothills of the central Himalayas, with valley floor at an average altitude of 1300 m a.s.l. The mountains surrounding the valley have peaks ranging from 2000 to 2800 m a.s.l. Neighboring valleys to the west, north, northeast and south have substantially lower elevations. The Kathmandu Valley's meteorology is influenced by large scale features, western disturbances and the South Asian Summer Monsoon, as well as local mountain-valley circulations. As reported by Panday and Prinn (2009) and Panday et al. (2009) during the dry season the diurnal cycle of air pollutants (CO, O_3, PM_{10}) is strongly affected by local meteorology connected to the evolution of the convective planetary boundary layer (PBL) and thermal wind flows along the flanks of the mountains surrounding the valley.

The Paknajol site is located (27°43'4" N, 85°18'32" E, 1380 m a.s.l.) near the edge of Kathmandu's tourist district of Thamel. The sampling site stands on the terrace (about 25 m a.g.l.) of the Ev-K2-CNR representative office. This is the highest building in the block, thus having a 360° free horizon of at least 300 m. The instruments are located in an air-conditioned room, in order to maintain the correct operating conditions; an UPS for uninterruptible power supply guarantees the continuous measurements in case of (frequents) blackout events, up to 18 hours a day power cut, especially during the winter months. The sampling heads are placed on the roof just outside this

room. The measurement activities, including aerosol and trace gas measurements, were started on February 2013.

The following instruments are used for continuous measurements:

1. UV-absorption analyser (TEI 49i, Thermo Environmental) is used to collect surface O_3 measurements. These are referred to the WMO/GAW reference scale (SRP#15, see Klausen et al., 2003) hosted at the GAW World Calibration Centre (WCC) at EMPA (Switzerland), via direct comparison with the CNR-ISAC laboratory standard hosted at the Mt. Cimone WMO/GAW Global Station (Italy). The experimental setup is similar to that described in Cristofanelli et al. (2010).
2. Aerosol light absorption and BC, derived by using the mass absorption efficiency of 6.5 m^2 g^{-1}, are measured through a Multi-Angle Absorption Photometer (MAAP 5012, Thermo Electron Corporation). For more details, see Marinoni et al. (2010). The correction described in Hyvärinen et al. (2013) for the measurement artifact, affecting the instrument's accuracy at high BC concentrations, was applied. A PM_{10} cutoff size was used in the sampling head.
3. Meteorological parameters (atmospheric pressure and temperature, wind speed and direction, relative humidity and precipitation) are monitored using an automatic weather station (WXT 425, VAISALA). Global solar radiation is monitored with a pyranometer (CMP21, Kipp&Zonen).
4. Aerosol number concentration and size distribution (in the range 0.28 μm ≤ Dp < 10 μm, Dp being the geometric diameter of particles) are measured using an Optical Particle Counter (OPC Monitor, FAI Instruments), which uses laser light scattering technique (λ=780 nm). The OPC optical diameters (divided in 8 bins) are then converted into geometric diameters, assuming that particles are spherical. In order to minimize biases related to coincidence errors, but also to reduce relative humidity and dry aerosol particles, the air sample is subjected to a dilution process, whose dilution factor can be varied, by modifying the dilution flow rate (from 0 to 4 l/min).
5. On-line PM_{10} and PM_1 are measured (with a 24 h resolution), using the β–absorption technique, with a medium-volume (2.3 m^3/h) sampler (SWAM Dual Channel, FAI Instruments). The instrument is equipped with two 12V back-up batteries, in order to complete measurements in case of electricity power breaks. From April 1st 2013 a PM_1 sampling head has been installed, replacing the $PM_{2.5}$ one.

All measurements presented in this work refer to Nepal Standard Time (NST, UTC+05:45); data are stored and fully validated on a 1-min basis, then averaged to a common time base of 60 minutes, and expressed in STP (0 °C and 1013 hPa) conditions. With the purpose of aggregating

data to hourly average values, 50% data coverage criteria was used, i.e. at least 50% coverage of the data sampling period was required to give a 1-h average.

2.2 Back-trajectories calculation

In order to describe the synoptic-scale atmospheric circulation scenarios over the Kathmandu Valley and the surrounding region, the isentropic 5-days back-trajectories have been used, computed by the HYSPLIT model (Draxler and Hess, 1998) every 6 h (at 5:45, 11:45, 17:45 and 23:45 NST). With the aim of minimizing the effect of the complex topography and provide a description of the large-scale circulation in the free troposphere, calculations were initialized at 600 hPa. The model calculations are based on the GDAS meteorological field produced by the NCEP reanalysis data, with a horizontal resolution of 1°x1°. In order to aggregate the back-trajectories of common origin, and better characterize the synoptic-scale circulation occurring at Paknajol, a cluster aggregation technique (Draxler, 1999) has been applied to the back-trajectories. Basically, at each step of the process, the appropriate number of clusters was identified, based on the variations of several statistical parameters; by maximizing between-group variance and minimizing within-group variance, this methodology might identify similar air-mass back-trajectories and aggregate them.

2.3 Recurrent model analysis

To understand how photochemistry and dynamics affect the variation of O_3 mixing ratios and to comprehend the origin of elevated O_3 levels in the afternoon and evening hours during the pre-monsoon period, we used a recurrent neural network model. These models allow us to simulate the non-linear relationship between O_3 and meteorological parameters that are proxies of photochemistry and dynamics (Lönnblad et al., 1992; Elman, 1990). Considering the strong role of meteorological conditions and photochemistry on the variations of O_3 mixing ratios (Pudasainee et al., 2006; Di Carlo et al., 2007) and the fact that meteorological effects usually last for more than one day, the more complex architecture of the neural network that uses the recurrent approach takes into account the multi-day effect of meteorology, as well as diurnal boundary layer cycles (Biancofiore et al., 2015). The model uses the observed pressure, temperature, relative humidity, solar radiation, wind velocity and direction and BC concentrations as input to simulate the O_3 mixing ratio (Biancofiore et al., 2015). The inclusion of a sub-group of these proxies allows us to distinguish between the role of dynamics and that of photochemistry in the observed variations of O_3 mixing ratio.

3. Results

3.1 Meteorological characterization

The Paknajol area is strongly influenced by local traffic and urban emissions, as it is located near the edge of Kathmandu's tourist center, and near a major thoroughfare. Meteorological observations at the sampling site help in better describing the seasonal and diurnal variability of the air pollutants and SLCF/P in the Kathmandu Valley.

With the aim of identifying the regional transition of the monsoon seasonal regimes, we considered meteorological observations carried out at the Nepal Climate Observatory-Pyramid (NCO-P) station, located at 5079 m a.s.l. near Mt. Everest in the Himalayas. As shown by Bonasoni et al. (2010), the variability of meteorological parameters (i.e. relative humidity and meridional wind component) observed at NCO-P can be used to derive the onset and withdrawal dates of the different seasons on the south side of the Himalayan range (where NCO-P is located). Moreover, as described in the annual report of the India Meteorological Department (IMD, 2014), the seasonal advance of the South Asian monsoon cycle did not differ too much between NCO-P location and Kathmandu. Table 1 reports the start and withdrawal dates of each season (pre-monsoon, monsoon, post-monsoon, winter) for the period considered in this study.

Figure 1 shows the variability of the meteorological parameters measured at Paknajol from February 2013 to the end of January 2014. Hourly atmospheric temperature (T, panel *a*) values never exceeded 29.5 °C, while minima never dropped below 3.5 °C. Over the whole measurement period, T had an average value of 18.7 ± 5.6 °C (hereinafter, average values are indicated as average ± one standard deviation). T was characterized by an evident diurnal cycle, with values peaking in the central part of the day and a minimum in the early morning. Atmospheric pressure (P, panel *b*, average value: 865.3 ± 4.1 hPa) showed its minimum values during the summer season, which is characterized by the presence of the monsoon trough over Nepal, accompanied by frequent and intense showers, reaching up to 47 mm/h (panel *d*). P is characterized by a semi-diurnal cycle, with two minima (at 4:00 and 16:00) and two maxima (at 10:00 and 22:00) with average amplitudes ranging from 1.2 hPa (pre-monsoon) to 3.5 hPa (post-monsoon). Relative humidity values (RH, panel *c*, average value: 67.1 ± 17.0 %) were high during all of the measurement period, rarely decreasing below 20% (50% during the summer monsoon season); it has to be noted that, during winter, RH values swing from very high to very low, thus presenting the widest diurnal cycle among all of the seasons. Saturation conditions (RH equal to 95% or higher) were mainly reached during the most intense rainfalls. In agreement with rainfall reported in Panday and Prinn (2009), about 90% of annual rainfall was observed during June-August. Panels *e* and *f* show wind speed and direction, respectively. The sampling site was characterized by low wind speeds, with majority of

winds from the W-NW sector, with secondary contribution from the W-SW sector (see Fig. S1, Supplementary Material). As shown in Panday and Prinn (2009) and Panday et al. (2009), nights were characterized by low wind speeds (maximum speed: 4 m/s) coming from several directions, mainly explained by katabatic winds descending from the mountain slopes at the edge of the Kathmandu Valley rim; on the other hand, during the afternoon, stronger winds (reaching up to 6.5 m/s) occurred at the measurement site, which was swept by westerly/northwesterly winds entering through the western passes.

3.2 SLCF/P seasonal and diurnal cycle

The hourly average (along with daily averages) time series for O_3, BC and particle number concentration are shown in Fig. 2. Figure 3 shows the diurnal variability of these pollutants across the seasons, while seasonal average values are presented in Table 2.

Similarly to other polluted cities, the rush hours and PBL dynamics result in the distinct morning and evening peaks: increase in traffic activities and congestion, increase in emissions from cooling/heating activities (LPG, kerosene and firewood), as well as decrease in PBL. The primary emission indicators, i.e. BC and aerosol particle number, reveal such activities. Industries, especially brick kilns, and open garbage burning also contribute to poor air quality in the Kathmandu Valley.

The average value of BC (Fig. 2, panel *a*) over the whole measurement period was 11.6 ± 10.7 $\mu g/m^3$. The highest BC concentrations were observed during pre-monsoon and winter seasons (Table 2), with daily values often exceeding 20 $\mu g/m^3$, while the lowest values occurred during the monsoon season (the lowest daily value recorded was 2.5 $\mu g/m^3$). These levels are slightly higher than what is reported in a previous study by Sharma et al. (2012) at Pulchowk Campus, in which they reported an average BC of 8.4 ± 5.1 $\mu g/m^3$, over a year-long study period spanning between May 2009 and April 2010. Another study by Shrestha et al. (2010) reported far lower values of EC concentration (1.7 ± 0.6 $\mu g/m^3$) for an urban site 30 km southeast (downwind) of the Kathmandu Valley, during the 2009 pre-monsoon season. The highest seasonal values, observed during winter/pre-monsoon, can be attributed to several factors: increase in emissions from domestic heating, use of small but numerous gensets during extended hours with power cuts, operation of over 100 brick kilns in the Valley, refuse burning, as well as lower PBL and lower wet deposition of pollutants in winter months compared to the summer months with intense heat and rainfall. The average diurnal variation in BC concentrations in the different seasons is shown in Fig. 3, panel a. The typical diurnal variation for BC, as also shown in Sharma et al. (2012), reflects the BC profile for an urban site, presenting two daily maxima, with a prominent peak in the morning (between

7:00 and 8:00), and a second one in the evening (between 20:00 and 21:00), as well as two minima at night (between 1:00 and 2:00) and in the afternoon (between 14:00 and 15:00). These two daily peaks reveal the start and build-up of emissions due to local anthropogenic activities, such as traffic and cooking activities. Moreover, also a meteorological component cannot be ignored: this is due to the presence of katabatic winds that lead to the uplift of surface polluted air-masses during the night. The following build-up of the morning mixed layer favors the downward mixing of pollutants back to the valley's bottom (Panday and Prinn, 2009; Panday et al., 2009). This diurnal cycle was observed in all four seasons but the peak values were much higher in winter and pre-monsoon seasons (morning peaks: 41.4 and 33.3 $\mu g/m^3$, respectively) compared to the post-monsoon and monsoon seasons (12.9 and 11.4 $\mu g/m^3$, respectively).

Surface ozone (O_3) had an average value of 27.0 ± 21.3 nmol/mol (1 nmol/mol is equivalent to 1 ppb) over the whole measurement period (Fig. 2, panel *b*). The highest O_3 was observed during the pre-monsoon season, while the lowest values were reached during the winter season (Table 2). This spring "peak" is a feature widely present on South Asia and Himalayas (see e.g. Cristofanelli et al., 2010; Agrawal et al., 2008). Pudasainee et al. (2006), with measurements made at Lalitpur, an adjacent city to the Kathmandu municipality, suggested that variations of solar radiation, ambient temperature and precursors (such as NOx and VOCs) can together explain 93% of the variation in measured ground level O_3 at Kathmandu. Following Chevalier et al. (2007), with the aim of attributing the fraction of O_3, BC, accumulation and coarse particles variability related to day-to-day and diurnal scale processes, we calculated the ratio of daily/hourly standard deviations. The obtained values (0.54 for O_3, 0.59 for BC, 0.81 for accumulation and 0.71 for coarse particles) indicated that both diurnal and day-to-day variations are important to explain O_3, BC and particle number variations at Paknajol. O_3 diurnal variation is shown in panel *b* of Fig. 3: a peak in O_3 mixing ratios characterized the central part of the day (between 11:00 and 13:00), while a minimum was observed in the morning (between 5:00 and 6:00). This diurnal variation is typical for polluted urban sites (Jacobson, 2002) and can be explained in terms of local O_3 photochemistry production and removal processes as well as PBL dynamic and vertical air-mass mixing, as discussed in Sect. 3.4.

Particle number concentrations of accumulation (0.28 μm ≤ Dp < 1 μm) and coarse (1 μm ≤ Dp < 10 μm) particles are reported in Fig. 2 (panels c and d, respectively). Unfortunately, due to instrumental failures, no measurements were available after July 27th, 2013: only two seasons were covered, i.e. pre-monsoon and monsoon. The average values over the available time period were 505 ± 372 cm^{-3} for the accumulation particles and 3.3 ± 2.4 cm^{-3} for the coarse particles. Accumulation and coarse particle concentrations were high during the pre-monsoon season and far

lower during the monsoon (Table 2). The average seasonal diurnal cycles (Fig. 3*c* for accumulation and 3*d* for coarse) were somewhat similar to that of BC, presenting two daily peaks, in correspondence to the start of working activities and traffic rush, thus indicating common anthropogenic emission sources and similar meteorological influences. The similar behavior between accumulation and coarse particle number concentrations suggests likely common origins, indicating that the main fraction of coarse particle is linked to the resuspension of road dust or ash from local combustion and not to mineral dust transport from desert areas. During the pre-monsoon, the morning peak was higher (1054 cm^{-3} for accumulation and 7.4 cm^{-3} for coarse) than the one recorded in the evening (629 cm^{-3} and 4.3 cm^{-3}, respectively). The same was true for the accumulation mode even during the monsoon season, although the difference between the two peaks showed smaller amplitude. For coarse particles, however, the evening peak appeared to be higher than the morning peak during the wet season. This can be explained by considering the wet conditions which usually characterized Kathmandu during night-time along this season; moreover, it has to be noted that this phenomenon may be combined to a not sufficient aerosol drying from the dilution system of the OPC. Most of the rain occurs during the night-time and the wet surface in the early morning prevents emission of roadside dust and soil. As the day evolves, moisture is more efficiently evaporated, leaving dry dust and soil to be resuspended by traffic or winds, thus leading to the appearance of a larger evening peak for coarse particle number.

Figure 4 shows the seasonal box and whiskers plot for PM_{10} and PM_1 collected at Paknajol. Prior to April 1st 2013, a $PM_{2.5}$ sampling head was installed in place of the PM_1 one. By considering the whole sampling period, PM_{10} had an average value of 169 ± 113 $\mu g/m^3$, which is comparable to the value found by Giri et al. (2006), 133.7 ± 70.3 $\mu g/m^3$, computed over the period 2003-2005 for the Thamel measurement site (not far from Paknajol), or to the values found in Aryal et al. (2008), which range from 170 to 230 $\mu g/m^3$ (annual averages) for two busy traffic area stations in Kathmandu. Our value appears slightly higher than those of Giri et al. (2006). This is in line with the increasing urbanization and vehicles growth which occurred in the Kathmandu Valley. The maximum seasonal average of PM_{10} was found during winter, while minima occurred during monsoon and post-monsoon seasons (Table 2). $PM_{2.5}$ presented an average value of 195 ± 83 $\mu g/m^3$ over its short time period (17 days), while PM_1 had an average value of 48 ± 42 $\mu g/m^3$, with the maximum values during the pre-monsoon and winter seasons and significantly lower values during monsoon and post-monsoon (Table 2). Over the whole measurement period, the ratio PM_1/PM_{10} was 0.29 ± 0.10, indicating a large contribution of coarse particles to the total aerosol mass. This aerosol mass concentration ratio, which values were the highest during the pre-monsoon (0.39 ± 0.09) and lowest during winter (0.21 ± 0.05), is similar to those observed for arid sites (Shahsavani

et al., 2012; Lundgren et al., 1996), for sites affected both by dust storm originating in Asia (Claiborn et al., 2000) and strong African dust outbreak episodes (Alastuey et al., 2005) and dusty roads (Colbeck et al., 2011). Similar ratios were observed also in other large municipalities in South Asia, such as Bilaspur (0.24, Deshnukh et al., 2010) or Raipur (0.28, Deshmukh et al., 2013) in India, or Nanjing (0.34, Wang et al., 2003) in China. In the European cities this ratio is generally higher than in Asia.

3.3 SLCF/P behavior as a function of wind direction

We highlighted the wind sector which mostly contributed to the occurrence of high SLCF/P values at the measurement site, as presented in Fig. 5. Here, the angular distribution of the pollutants averaged over WD intervals of 10° (green lines) is shown. Also reported in the figure are the distributions of the frequency of wind directions (blue) and the relative abundance of the pollutants (red), weighted by the wind directions, computed according to Gilge et al. (2010). These analyses refer to the whole investigation period and no significant differences were observed by categorizing data as a function of the different seasons, nor time of day. WD behavior has already been presented in Sect. 3.1; BC and aerosol particle number (both accumulation and coarse) average values did not show any dependence as a function of wind direction: this is conceivable considering that Paknajol is located in the middle of several pollution sources. O_3 angular mean values (green line) showed enhanced values from W-NW sector (35 nmol/mol on average). This leads to a small distortion of the O_3 contribution away from the distribution of the wind directions (peaking at 270°) and 48% of the total O_3 recorded at Paknajol station was enclosed in the 240-320° wind sector, which perfectly matches the direction from a mountain pass from where, according to Panday and Prinn (2009), air-masses can be transported during day-time towards Kathmandu due to thermal transport, indicating arrival of regional polluted air-masses.

3.4 Correlation analysis among SLCF/P

By looking at the diurnal variations presented in Fig. 3, the first peak in BC and aerosol particles can be explained in terms of increased emission (traffic and cooking activity) under atmospheric stable conditions and low PBL height or with an additional contribution of down-mixing as the night-time stable boundary layer breaks up (Panday and Prinn, 2009). Dilution within the higher PBL, arrival of cleaner air from west of the Kathmandu Valley, and decrease of emissions can explain the daily minimum in aerosol and BC observed from 11:00 to 17:00. Conversely, the peak in O_3 can be explained in terms of enhanced photochemical production (with respect to night-time or early morning), as well as downward vertical mixing of polluted regional air-masses from the

free troposphere or the night-time residual layer. When the PBL height starts to decline due to the diurnal decrease of solar radiation and soil heating, along with the increased emissions of the evening traffic and cooking activities, a secondary peak in BC aerosol is observed from 18:00 to 22:00. Titration with NO, dry deposition and less efficient vertical mixing within a more stable PBL lead to the decrease of O_3 which finally results in the night-time minimum, when BC and aerosol particles also present the lowest concentrations due to the decrease of traffic and domestic emissions. Moreover, since measurements were taking place on the roof of a tall building, in presence of a stable night-time atmosphere it may be difficult to capture near surface pollution. These behaviors led to a negative correlation between hourly BC and O_3 (Table 3), which was almost constant over all of the considered seasons. The O_3 decrease after the noon peak was faster during winter and post-monsoon seasons, while it was more gradual during pre-monsoon and monsoon. Moreover, during the pre-monsoon season, a "bump" in O_3 mixing ratios (>50 nmol/mol) was observed during the afternoon (between 11:00 and 17:00, Fig. 3). The simultaneous decreases of BC and aerosol particle concentrations support a strong role of downward vertical mixing in enhancing O_3 and decreasing primary pollutants (BC and aerosol particles). The important role of dynamics in influencing SLCF/P variability is confirmed by the negative (positive) correlation between wind speed and BC (O_3). The correlation coefficients (r) are higher by considering daily average values (Table 3), supporting the role of day-to-day meteorology in influencing the SLCF/P.

BC showed significantly higher hourly correlation with accumulation and coarse particles (0.86 and 0.87, respectively), which was lower during the wet season (0.66), strongly supporting common sources and processes influencing their variability (i.e. traffic sources and PBL dynamics). The lower correlation can be explained in terms of different hygroscopicity of BC with respect to other aerosol particles (see Marinoni et al., 2010), which can lead to lower scavenging efficiency of BC with respect to other inorganic and organic species that has been proved especially for not aged BC (Cozic et al., 2007). Due to the lack of data, no information about the variation of the correlation coefficients computed between accumulation and coarse particles could be given other than during pre-monsoon and monsoon seasons. The high correlation coefficient between BC and accumulation (and coarse) particle could however indicate that BC can be used as an indicator of primary pollution, even when measurements by the OPC are lacking.

O_3 showed high correlation with solar radiation (0.71 for hourly and 0.56 for daily values) and temperature, considered as a proxy for season (0.51 and 0.32): this is somewhat expected for an urban site like Kathmandu, where photochemistry and PBL dynamics (indirectly driven by solar radiation and temperature behavior) play an important role in determining O_3 variability (Pudasainee et al., 2006). The correlation with solar radiation exhibited some variability during the

year, giving the lowest values (0.59 for hourly and 0.06 for daily values) during the pre-monsoon season, possibly supporting the enhanced role of atmospheric transport and dynamics in influencing O_3 with respect to photochemistry. Apparently, this agrees only in part with the results shown in Pudasainee et al. (2006), in which the authors argued that the "flat peak" in O_3 concentrations during the pre-monsoon is mainly due to abundance of solar radiation and higher temperature (justified by high correlation coefficient values).

In order to distinguish the chemical effects from the boundary layer dynamics, we also computed correlation coefficients limiting the data to convective hours only (i.e. between 11:00 and 17:00, according to the wind speed and solar radiation diurnal variations). The slightly weaker correlation between BC and accumulation particle number and, on the other hand, the increase in correlation between O_3 and accumulation particle number may indicate the role of other processes (e.g. secondary aerosol production) occurring in the air-masses which characterize this specific time span (Table S1, Supplement). In particular, we suppose that aged air-masses rich in secondary pollutants (i.e. O_3 and aerosol) can be transported to the measurement site in the afternoon mixed layer.

Here, we argue that mixing processes with upper residual O_3 layers can explain this behavior. Sensitivity tests with a recurrent neural network model, using different subgroups of proxies, have been carried out and the results are shown in Fig. 6, where the observed and different simulated average diurnal O_3 mixing ratios are compared. The simulation that included all the proxies reproduced quite well the observed O_3 mixing ratios for all hours of the day, whereas a simulation that included only wind speed (a good proxy of atmospheric dynamics) reproduced with accuracy the afternoon (after 15:00) and evening levels of O_3, missing completely the main O_3 peak before noon. In contrast, by using as input parameters both wind speed and solar radiation, the model reproduced well the peak before noon and the high levels of afternoon-evening O_3. Putting together the results of these two simulations, we can conclude that the high level of O_3 during the afternoon is mainly due to dynamics (vertical intrusion from upper atmospheric layers and/or horizontal advection), for the following two reasons: (i) in the model, the wind speed used as input is enough to reproduce the afternoon concentrations of O_3 and (ii) the inclusion of solar radiation does not improve the agreement between measured and modelled O_3 during the afternoon, but substantially enhances the agreement between measurements and simulations before noon, when photochemistry, as expected, plays a larger role. The photochemistry contribution varied as a function of the hour of the day, ranging from 6% to 34%.

3.5 Influence of atmospheric synoptic circulation

3.5.1 Synoptic-scale air-mass circulation scenarios

With the purpose of investigating the variability of large-scale atmospheric circulation affecting the region of interest, we clustered the HYSPLIT 5-days back-trajectories. Here, it should be clearly stated that this analysis has been carried out with the aim of providing information about the synoptic-scale circulation scenarios which affect the region where the Kathmandu Valley is located and therefore investigating the link among these scenarios with the SLCF/P variability. In order to retain robust information, only the days for which the same cluster was observed for at least ¾ of daily observations were considered in this analysis. Overall, 9 clusters were identified; Figure 7 shows the percentage of occurrence for each cluster for the whole investigation period, as a function of the different seasons. 3 clusters out of 9 had a very small percentage of occurrences (i.e. less than 5% of air-masses for each of these clusters were recorded), thus were not retained for further analysis (see Supplementary Material). "Regional" (REG, 21.9%) and "Western" (WES, 21.4%) clusters showed the highest occurrence values. The first encompasses trajectories within a 10°x10° area centered on the region of interest, thus indicating the occurrence of regional-scale atmospheric circulation: trajectories from this area were present in every season, except winter. WES, on the other hand, represents westerly air-masses which originated (5-days backward in time) at a longitude around 60° E. The cyclonic behavior of these back-trajectories indicated that synoptic-scale westerly disturbances could steer air-masses under these scenarios. A significant fraction of trajectories (16.3%), mostly observed during pre-monsoon and winter, showed again westerly transport at synoptic-scale (even if presenting higher horizontal velocities with respect to WES): 5-day back-trajectories originated or travelled over desert areas of Arabian Peninsula (ARAB-PEN). The larger latitudinal span of these back-trajectories suggested that synoptic-scale disturbances and subtropical jet stream latitudinal excursions could steer the air-masses towards the region of interest. During the monsoon and post-monsoon seasons, the atmospheric circulation was strongly affected by the summer monsoon and by the occurrence of low pressure areas in the Bay of Bengal, which enhanced the possibility to observe easterly circulation: i.e. "Bay of Bengal" (BENG, 12.8%) and "Eastern" (EAS, 14.8%) clusters. Finally, a not negligible fraction of days (5.6%, occurring mostly during winter) can be tagged to south-westerly circulation (SW), which can be related to the passage of synoptic-scale disturbances over the western Indian subcontinent (Böhner, 2006). For more details and plots concerning the different back-trajectory clusters, please see the Supplementary Material.

3.5.2 Influence of atmospheric circulation on O_3 and BC diurnal variations

The BC and O_3 diurnal variations, as a function of the different synoptic-scale air-mass circulation scenarios (Sect. 3.5.1) are shown in Fig. 8. The BC diurnal variation was only partly

dependent from the air-mass clusters: the shape was the same for all of the clusters, although a difference in the amplitude of the cycles was recorded. In particular, regional air-masses or on the eastern regions (BENG and EAS) were associated to smaller BC values both during peaks and minimum levels. This is because air-masses from these regions were retrieved only during monsoon and post-monsoon seasons, when BC concentrations were at their minimum (no occurrences at all were registered during winter) due to enhanced wash-out. On the other hand, during winter and pre-monsoon, the highest values of BC were recorded under ARAB-PEN, WES and SW air-mass circulation. Particularly, the diurnal cycle of BC and the relative 24-hour averaged peak values in the morning and in the evening were maximized when SW circulation affected the measurement site.

Concerning O_3 diurnal variation, significant differences can be observed as a function of different synoptic-scale circulation scenarios. Despite a moderate diurnal cycle of BC, the highest diurnal peak value and the largest amplitude of daily cycle were observed for the WES circulation: we can hypothesize that air-masses from the free troposphere or overpassing polluted regions above the Indo-Gangetic Plain could contribute in the appearance of these high values. It is interesting to note that for the three synoptic scale scenarios, most frequent during pre-monsoon and winter (i.e. WES, ARAB-PEN and SW), very different results were obtained for BC and O_3. In particular, the diurnal peaks were maximized (minimized) for O_3 (BC). This can be tentatively explained by suggesting that, under this circulation, meteorological conditions should favor the dilution of polluted air-masses emitted from surface sources and transport of O_3-rich upper layers by vertical entrainment processes (e.g. Kleinman et al., 1994). Similar diurnal cycles but lower mixing ratios were tagged to ARAB-PEN and REG circulations. As for BC, the smallest O_3 diurnal cycles were linked to the typical monsoon circulations EAS and BENG: this is in agreement with Agrawal et al. (2008) who indicated that, due to widespread rain precipitation and cloudy conditions, summer monsoon is not favorable to photochemical O_3 production and to the occurrence of elevated O_3 regime. With respect to other atmospheric circulation, the average O_3 diurnal cycles for ARAB-PEN, REG and WES were characterized by high values from 13:00 to 21:00, while an intermediate condition was observed for the SW circulation.

3.6 Influence of open vegetation fires on BC and O_3 values

As shown in Putero et al. (2014), the BC and O_3 values in Nepal are partly influenced by the emissions from open vegetation fires, occurring across broad regions. In order to evaluate the contribution of large open fires emissions to the BC and O_3 variations observed at Paknajol, the daily total number of fires by the MODIS product has been retrieved and used. Fire pixels (with a

confidence value ≥ 75%) were derived from the MODIS Global Monthly Fire Location Product (MCD14ML); these have been "filtered" by means of the MODIS Land Cover Climate Modeling Grid Product (MCD12C1), in order to retain only fires occurring over specific land use categories (i.e. vegetation, croplands, forests; for more details on such products, see Justice et al., 2002; Friedl et al., 2010). This methodology did not allow us to account for the fraction that came from "residential" burning (e.g. garbage burning occurring in urban areas, or domestic). The study area for the open vegetation fires occurrences was the Southern Himalayas box (26° N ≤ Lat ≤ 30° N; 80° E ≤ Lon ≤ 88° E) considered in Putero et al. (2014) as the main contributor for Nepal. Over the whole period, the correlation coefficient between the number of fires and the delayed (from t to t-3 days) BC concentrations showed almost null correlation (0.10), pointing out that, in general, the BC fraction could be mainly influenced by other (local) anthropogenic emissions, also including the contribution from domestic and garbage burning. A sensitivity study was carried out by considering slightly different spatial domains for the fire detection, without significant changes of the results. Nevertheless, some BC peaks have been superimposed to periods of high fire activities. During these events, the large-scale synoptic scenario, as deduced by HYSPLIT, showed WES and REG circulation, thus supporting the presence of regional-scale transport, and the possible influence from specific distinct (major) events of open vegetation fires. However, several limitations of the use of back-trajectories and MODIS data (which can miss short-time events, small fires, and fires under clouds) have to be taken into account; for this reason, the use of chemical transport modeling outputs would be required for investigating these events in deeper detail. Figure 9 shows the diurnal BC and O_3 variations for the period of study (panels *a*-*b*) and the time series of total daily fires over the Southern Himalayas box (as defined above) retrieved by MODIS (panel *c*).

BC diurnal variation seemed to remain pretty constant over the entire time period, thus suggesting no prominent influence by fire emissions. During high fire activity periods (e.g. during the pre-monsoon season), BC showed increased concentrations, even though no shift of the daily maxima position occurred, thus indicating that local emissions (traffic and/or domestic, including open garbage burning) and PBL dynamic are the main factors influencing BC concentrations at Paknajol, further supported by the high ratio BC/PM_1. The same could not be said considering O_3 measurements. When the number of fires was at the highest values, the O_3 peak was "shifted" in time and appeared in the late afternoon (between 16:00 and 18:00). This period almost perfectly matched with the "bump" in O_3 observed at diurnal scale during the pre-monsoon season (Sect. 3.4). Here we hypothesize that biomass burning plumes that were enriched in O_3 photochemically produced after enhanced emission of precursors (e.g. CO, VOCs) could be transported over

Kathmandu and possibly mixed within PBL due to efficient vertical mixing between upper ozone layers and surface layer.

4. Conclusions

In this work, we analyzed one full year of hourly-resolution data (February 2013 – January 2014) of SLCF/P (BC and O_3) as well as aerosol number and mass concentration, observed at Paknajol, an urban site in central Kathmandu city, Nepal. Very high values of SLCF/P were detected during the whole measurement period, indicating persistent poor air quality conditions, dangerous for the human health and the environment, including influence on local/regional climate.

Equivalent BC, aerosol number concentration and mass presented seasonal cycles with the highest values during winter and pre-monsoon and minima during the summer. Surface O_3 was characterized by maximum values during the pre-monsoon and a diurnal cycle (day-time maxima) opposite to what was observed for aerosol (mid-day minimum and maximum early in the morning and late evening). The diurnal behavior of BC and aerosol number concentration indicated that local pollution sources, mostly related to road traffic or domestic emissions, represent the major contribution to air pollution in Kathmandu.

Concerning O_3, the analysis of the seasonal change of the diurnal cycle and correlation with meteorological parameters and aerosol properties suggested that, apart from photochemistry (which contribution ranges from 6% to 34%), PBL dynamics and wind circulation have a significant role in determining its variability: during mid-day, air-masses richer in O_3 appeared to be transported to the measurement site by flows through the mountain passes located at the western rim of the Kathmandu valley. Especially during pre-monsoon, high O_3 values were observed during the afternoon. We suggest that mixing and vertical entrainment processes between upper layers and PBL could partially explain the occurrence of these high values and can lead to favorable conditions for O_3 production that will often result in exceedance of guideline values set by the World Health Organization (WHO).

The possible impact of emissions by major open vegetation fires occurring at regional scale has been assessed by analyzing MODIS fire distribution: a significant impact has been observed only for O_3 and during specific episodes, able to affect day-to-day variability. Despite the limitations of the methodology (e.g. garbage and domestic burning were not considered in this analysis and small or short-lasting open fires can be missed by satellite detection), this indicates that the occurrence of widespread biomass burning emissions can represent, in particular during the pre-monsoon season, a not-negligible source of precursors for O_3 photochemical production in the Kathmandu Valley.

The analysis of large-scale atmospheric circulation demonstrated a significant impact of the "background" synoptic-scale circulation on diurnal cycles of BC and O_3 in Kathmandu. In particular, atmospheric circulation related to westerly (WES, ARAB-PEN, SW) and regional (REG) circulations appeared to be especially conducive for the occurrence of the high BC and O_3 values.

Considering the 24 h limit of 120 μg/m^3 proposed for PM_{10} measurements from Government of Nepal (Giri et al., 2006), we found, for the 2013 period, a total of 124 exceedances, 51.4% of the available PM_{10} data. In 2003, the Nepali Ministry of Population and Environment (MoPE) has also defined five different quality descriptions (classes) based on PM_{10} levels (see HMG/MOPE, 2003). During our observation period, following these references, 12 days (5% of data) were categorized as "Good" (range 0-60 μg/m^3), 105 as "Moderate" (61-120 μg/m^3) and 103 days were tagged as "Unhealthy" (121-350 μg/m^3), representing 43.6% and 42.7% of data, respectively. A total of 21 days (8.7%) were classified as "Very Unhealthy" (351-425 μg/m^3, 13 days) or "Hazardous" (>425 μg/m^3, 8 days). Therefore, these data reveal the poor air quality in Kathmandu, also considering that the WHO guideline defines the limits of 20 μg/m^3 per year and 50 μg/m^3 per 24 hour. WHO (2006) also defined air quality guidelines for O_3 based on the analysis of the daily maximum 8-hour concentrations: High Levels (HL: 240 μg/m^3); Interim Target-1 (IT-1: 160 μg/m^3) and Air Quality Guideline (AQG: 100 μg/m^3). Based on Paknajol data, we found 13 days exceeding the IT-1 (3.5% of the data-set) and 125 days (34% of the data-set) exceeding the AQG. It should be noted that WHO associated "important health effects" to IT-1 exceedances, indicating that the exposures at the IT-1 level increases the number of attributable deaths by 3–5%. On the other side, the exceedances of the AQG are related to an estimated 1–2% increase in daily mortality (WHO, 2006). The totality of IT-1 exceedances were recorded during the pre-monsoon season, while AQG exceedances were observed for 62% during the pre-monsoon, 22% during the monsoon and the remaining during post-monsoon (4%) and winter (12%). Roughly, the total number (97%) of exceedances (IT-1 and AQG) were observed from 10:00 to 18:00. It is worth noting that 37 days (all detected during the pre-monsoon) were affected by the occurrence of major open vegetation fire activity during the investigated period. By neglecting these days, all of the IT-1 exceedances for O_3 at Paknajol were removed, and 88 AQG exceedances were retained (all the days with fire activity were tagged to AQG exceedances), representing a 29% (47%) decrease on a yearly (seasonal) basis.

The information of this study, developed in the framework of the SusKat-ABC project, may be useful for implementing control measures to mitigate the occurrence of acute pollution levels in the Kathmandu municipality, as well as for improving regional climate conditions, important for the wide area that lies at the foothills of the pristine Himalayan environment.

Acknowledgments

This work was supported by the National Project NextData, funded by the Italian Ministry of University and Research. The authors thank the Institute for Advanced Sustainability Studies (IASS) and the International Centre for Integrated Mountain Development (ICIMOD) that led the Sustainable Atmosphere for the Kathmandu Valley (SusKat) project. This study was partially supported by core funds of ICIMOD contributed by the governments of Afghanistan, Australia, Austria, Bangladesh, Bhutan, China, India, Myanmar, Nepal, Norway, Pakistan, Switzerland, and the United Kingdom.

References

Agrawal, M., Auffhammer, M., Chopra, U. K., Emberson, L., Iyngararasan, M., Kalra, N., Ramana, M. V., Ramanathan, V., Singh, A. K., and Vincent, J.: Impacts of Atmospheric Brown Clouds on agriculture, Part II of Atmospheric Brown Clouds: regional assessment report with focus on Asia, Project Atmospheric Brown Cloud, UNEP, Nairobi, Kenya, 2008.

Alastuey, A., Querol, X., Castillo, S., Escudero, M., Avila, A., Cuevas, E., Torres, C., Romero, P.-M., Exposito, F., Garcia, O., Diaz, J. P., Van Dingenen, R., and Putaud, J. P.: Characterisation of TSP and PM2.5 at Izaña and Sta. Cruz de Tenerife (Canary Islands, Spain) during a Saharan Dust Episode (July 2002), Atmos. Environ., 39, 4715-4728, 2005.

Aryal, R. K., Lee, B.-K., Karki, R., Gurung, A., Kandasamy, J., Pathak, B. K., Sharma, S., and Giri, N.: Seasonal PM_{10} dynamics in Kathmandu valley, Atmos. Environ., 42, 8623-8633, 2008.

Biancofiore, F., Verdecchia, M., Di Carlo, P., Tomassetti, B., Aruffo, E., Busilacchio, M., Bianco, S., Di Tommaso, S., and Colangeli, C.: Analysis of surface ozone using a recurrent neural network, Sci. Total Environ., 514, 379–387, 2015.

Böhner, J.: General climatic controls and topoclimatic variations in Central and High Asia, Boreas, 35, 279-294, 2006.

Bonasoni, P., Laj, P., Marinoni, A., Sprenger, M., Angelini, F., Arduini, J., Bonafè, U., Calzolari, F., Colombo, T., Decesari, S., Di Biagio, C., di Sarra, A. G., Evangelisti, F., Duchi, R., Facchini, M.C., Fuzzi, S., Gobbi, G. P., Maione, M., Panday, A., Roccato, F., Sellegri, K., Venzac, H., Verza, G.P., Villani, P., Vuillermoz, E., and Cristofanelli, P.: Atmospheric Brown Clouds in the Himalayas: first two years of continuous observations at the Nepal Climate Observatory-Pyramid (5079 m), Atmos. Chem. Phys., 10, 7515-7531, 2010.

Chevalier, A., Gheusi, F., Delmas, R., Ordonez, C., Sarrat, C., Zbinden, R., Thouret, V., Athier, G., and Cousin, J.-M.: Influence of altitude on ozone levels and variability in the lower

642 troposphere: a ground-based study for western Europe over the period 2001-2004, Atmos.
643 Chem. Phys., 7, 4311-4326, 2007.
644 Claiborn, C. S., Finn, D., Larson, T. V., and Koenig, J. Q.: Windblown dust contributes to high
645 PM2.5 concentrations, J. Air Waste Ma., 50 (8), 1440-1445, 2000.
646 Colbeck, I., Nasir, Z. A., Ahmad, S., and Ali, Z.: Exposure to PM10, PM2.5, PM1 and Carbon
647 Monoxide on roads in Lahore, Pakistan, Aerosol Air Qual. Res., 11, 689-695, 2011.
648 Cozic, J., Verheggen, B., Mertes, S., Connolly, P., Bower, K., Petzold, A., Baltensperger, U., and
649 Weingartner, E.: Scavenging of black carbon in mixed phase clouds at the high alpine site
650 Jungfraujoch, Atmos. Chem. Phys., 7, 1797-1807, 2007.
651 Cristofanelli, P., Bracci, A., Sprenger, M., Marinoni, A., Bonafè, U., Calzolari, F., Duchi, R., Laj,
652 P., Pichon., J.M., Roccato, F., Venzac, H., Vuillermoz, E. and Bonasoni, P.: Tropospheric
653 ozone variations at the Nepal Climate Observatory-Pyramid (Himalayas, 5079 m a.s.l.) and
654 influence of deep stratospheric intrusion events, Atmos. Chem. Phys., 10, 6537-6549, 2010.
655 Deshmukh, D. K., Deb, M. K., and Verma, S. K.: Distribution patterns of coarse, fine and ultrafine
656 atmospheric aerosol particulate matters in major cities of Chhattisgarh. Indian J. Environ.
657 Prot., 30, 184-197, 2010.
658 Deshmukh, D. K., Deb, M. K., and Mkoma, S. L.: Size distribution and seasonal variation of size-
659 segregated particulate matter in the ambient air of Raipurcity, India, Air Qual. Atmos.
660 Health, 6, 259-276, 2013.
661 Di Carlo, P., Pitari, G., Mancini, E., Gentile, S., Pichelli, E., and Visconti, G.: Evolution of surface
662 ozone in central Italy based on observations and statistical model, J. Geophys. Res., 112,
663 D10316, doi: 10.1029/2006JD007900, 2007.
664 Draxler, R. R., and Hess, G. D.: An overview of the HYSPLIT_4 modelling system for trajectories,
665 dispersion and deposition, Aust. Meteorol. Mag., 47, 295-308, 1998.
666 Draxler, R. R.: HYSPLIT4 user's guide. NOAA Tech. Memo. ERL ARL-230, NOAA Air
667 Resources Laboratory, Silver Spring, MD, 1999.
668 Elman, L. J.: Finding structure in time, Cognitive Sci., 14, 179–211, 1990.
669 Faiz, A., Ale, B. B., and Nagarkoti, R. K.: The role of inspection and mainteinance in controlling
670 vehicular emissions in Kathmandu Valley, Nepal, Atmos. Environ., 40, 5967-5975, 2006.
671 Friedl, M. A., Sulla-Menashe, D., Tan, B., Schneider, A., Ramankutty, N., Sibley, A., and Huang,
672 X.: MODIS Collection 5 global land cover: algorithm refinements and characterization of
673 new datasets, Remote Sens. Environ., 114, 168-182, 2010.

Gilge, S., Plass-Duelmer, C., Fricke, W., Kaiser, A., Ries, L., Buchmann, B., and Steinbacher, M.: Ozone, carbon monoxide and nitrogen oxides time series at four alpine GAW mountain stations in central Europe, Atmos. Chem. Phys., 10, 12295-12316, 2010.

Giri, D., Murthy, K., Adhikary, P. R., and Khanal, S. N.: Ambient air quality of Kathmandu valley as reflected by atmospheric particulate matter concentrations (PM_{10}), Int. J. Environ. Sci. Te., 3 (4), 403-410, 2006.

HMG/MOPE: Draft report on air emission inventory, Kathmandu, Nepal, 2003.

Hyvärinen, A.-P., Vakkari, V., Laakso, L., Hooda, R. K., Sharma, V. P., Panwar, T. S., Beukes, J. P., van Zyl, P. G., Josipovic, M., Garland, R. M., Andreae, M. O., Pöschl, U., and Petzold, A.: Correction for a measurement artifact of the Multi-Angle Absorption Photometer (MAAP) at high black carbon mass concentration levels, Atmos. Meas. Tech., 6, 81-90, 2013.

India Meteorological Department (IMD): Monsoon report 2013. Edited by Pai, D S, and Bhan S C. Pune, India, 2014.

Jacobson, M. Z.: Atmospheric pollution: history, science and regulation, Cambridge University Press, Cambridge, United Kingdom and New York, NY, USA, 2002.

Justice, C. O., Giglio, L., Korontzi, S., Owens, J., Morisette, J. T., Roy, D., Descloitres, J., Alleaume, S., Petitcolin, F., and Kaufman, Y.: The MODIS fire products, Rem. Sens. Environ., 83, 244-262, 2002.

Klausen, J., Zellweger, C., Buchmann, B., and Hofer, P.: Uncertainty and bias of surface ozone measurements at selected Global Atmosphere Watch sites, J. Geophys. Res., 108 (D19), 4622, doi:10.1029/2003JD003710, 2003.

Kleinman, L., Lee, Y.-N., Springston, S. R., Nunnermacker, L., Zhou, X., Brown, R., Hallock, K., Klotz, P., Leahy, D., Lee, J. H., and Newman, L.: Ozone formation at a rural site in the southeastern United States, J. Geophys. Res., 99 (D2), 3469-3482, 1994.

Lönnblad, L., Peterson, C., Röngvalsson, T.: Pattern recognition in high energy physics with artificial neural network — Jetnet 2.0, Comput. Phys. Commun., 70, 167–182, 1992.

Lundgren, D. A., Hlaing, D. N., Rich, T. A., and Marple, V. A.: PM10/PM2.5/PM1 data from a trichotomous sampler, Aerosol Sci. Tech., 25 (3), 353-357, 1996.

Marinoni, A., Cristofanelli, P., Laj, P., Duchi, R., Calzolari, F., Decesari, S., Sellegri, K., Vuillermoz, E., Verza, G.P., Villani, P. and Bonasoni, P.: Aerosol mass and black carbon concentrations, a two year record at NCO-P (5079 m, Southern Himalayas), Atmos. Chem. Phys., 10, 8551-8562, 2010.

Monks, P. S., Granier, C., Fuzzi, S., Stohl, A., Williams, M. L., Akimoto, H., Amann, M., Baklanov, A., Baltensperger, U., Bey, I., Blake, N., Blake R. S., Carslaw, K., Cooper O. R., Dentener, F., Fowler, D., Fragkou, E., Frost, G. J., Generoso, S., Ginoux, P., Grewe, V., Guenther, A., Hansson, H. C., Henne, S., Hjorth, J., Hofzumahaus, A., Huntrieser, H., Isaksen, I. S. A., Jenkin, M. E., Kaiser, J., Kanakidou, M., Klimont, Z., Kulmala, M., Lawrence, M. G., Lee, J. D., Liousse, C., Maione, M., and McFiggans, G.: Atmospheric composition change – global and regional air quality, Atmos. Environ., 43, 5268-5350, 2009.

Panday, A., and Prinn, R. G.: Diurnal cycle of air pollution in the Kathmandu Valley, Nepal: Observations, J. Geophys. Res., 114, D09305, doi:10.1029/2008JD009777, 2009.

Panday, A., Prinn, R. G., and Schär, C.: Diurnal cycle of air pollution in the Kathmandu Valley, Nepal: 2. Modeling results, J. Geophys. Res., 114, D21308, doi: 10.1029/2008JD009808, 2009.

Pudasainee D., Balkrishna S., Shrestha, M. L., Kaga, A., Kondo, A., and Inoue, Y.: Ground level ozone concentrations and its association with NOx and meteorological parameters in Kathmandu valley, Nepal, Atmos. Environ., 40, 8081-8087, 2006.

Putero, D., Landi, T. C., Cristofanelli, P., Marinoni, A., Laj, P., Duchi, R., Calzolari, F., Verza, G. P., and Bonasoni, P.: Influence of open vegetation fires on black carbon and ozone variability in the southern Himalayas (NCO-P, 5079 m a.s.l.), Environ. Pollut., 184, 597-604, 2014.

Ramanathan, V., Li, F., Ramana, M. V., Praveen, P. S., Kim, D., Corrigan, C. E., Nguyen, H., Stone, E. A., Schauer, J. J., Carmichael, G. R., Adhikary, B., and Yoon, S. C.: Atmospheric brown clouds: Hemispherical and regional variations in long-range transport, absorption, and radiative forcing, J. Geophys. Res., 112, D22S21, doi: 10.1029/2006JD008124, 2007.

Ramanathan, V., and Carmichael, G.: Global and regional climate changes due to black carbon, Nat. Geosci., 1, 221-227, 2008.

Rupakheti, M., Panday, A. K., Lawrence, M. G., Kim, S. W., Sinha, V., Kang, S. C., Naja, M., Park, J. S., Hoor, P., Holben, B., Bonasoni, P., Sharma, R. K., Mues, A., Mahata, K., Bhardwaj, P., Sarkar, C., Rupakheti, D., Regmi, R. P., and Gustafsson, Ö.: Air pollution in the Himalayan foothills: Overview of the SusKat-ABC international air pollution measurement campaign in Nepal, To be submitted to Atmos. Chem. Phys., 2015.

Shahsavani, A., Naddafi, K., Jafarzade Haghighifard N., Mesdaghinia, A., Yunesian, M., Nabizadeh, R., Arahami, M., Sowlat, M. H., Yarahmadi, M., Saki, H., Alimohamadi, M., Nazmara, S., Motevalian, S. A., and Goudarzi, G.: The evaluation of PM10, PM2.5 and

741 PM1 concentrations during the Middle Eastern Dust (MED) events in Ahvaz, Iran, from
742 april through September 2010, J. Arid Environ., 77, 72-83, 2012.
743 Sharma, C. K.: Urban air quality of Kathmandu Valley "Kingdom of Nepal", Atmos. Environ., 31
744 (17), 2877-2883, 1997.
745 Sharma, R. K., Bhattarai, B. K., Sapkota, B. K., Gewali, M. B., and Kjeldstad, B: Black carbon
746 aerosols variation in Kathmandu valley, Nepal, Atmos. Environ., 63, 282-288, 2012.
747 Shindell, D., Kuylenstierna, J. C. I., Vignati, E., van Dingenen, R., Amann, M., Klimont, Z.,
748 Anenberg, S. C., Muller, N., Janssens-Maenhout, G., Raes, F., Schwartz, J., Faluvegi, G.,
749 Pozzoli, L., Kupiainen, K., Höglund-Isaksson, L., Emberson, L., Streets, D., Ramanathan,
750 V., Hicks, K., Kim Oanh, N. T., Milly, G., Williams, M., Demkine, V., and Fowler, D.:
751 Simultaneously mitigating near-term climate change and improving human health and food
752 security, Science, 335, 183-189, 2012.
753 Shrestha, P., Barros, A. P., and Khlystov, A.: Chemical composition and aerosol size distribution of
754 the middle mountain range in the Nepal Himalayas during the 2009 pre-monsoon season,
755 Atmos. Chem. Phys., 10 (23), 11605-11621, 2010.
756 Shrestha, R. M. and Malla, S.: Air pollution from energy use in a developing country city: the case
757 of Kathmandu Valley, Nepal, Energy, 21 (9), 785-794, 1996.
758 Shrestha, R. M., and Rajbhandari, S.: Energy and environmental implications of carbon emission
759 reduction targets: Case of Kathmandu Valley, Nepal, Energ. Policy, 38 (9), 4818-4827,
760 2010.
761 Shrestha, S. R., Kim Oanh, N. T., Xu, Q., Rupakheti, M., and Lawrence, M. G.: Analysis of the
762 vehicle fleet in the Kathmandu Valley for estimation of environment and climate co-benefits
763 of technology intrusions, Atmos. Environ., 81, 579-590, 2013.
764 UNEP and WMO: Integrated Assessment of Black Carbon and Tropospheric Ozone, UNEP,
765 Nairobi, 2011.
766 Wang, G., Wang, H., Yu, Y., Gao, S., Feng, J., Gao, S., and Wang, L.: Chemical characterization of
767 water-soluble components of PM10 and PM2.5 atmospheric aerosols in five locations of
768 Nanjing, China, Atmos. Environ., 37, 2893-2902, 2003.
769 World Health Organization: WHO Air quality guidelines for particulate matter, ozone, nitrogen
770 dioxide and sulfur dioxide, Global update 2005, Summary of risk assessment, WHO Press,
771 Geneva, Switzerland, 2006.
772

Table 1. Onset and decay dates of the different seasons selected in this work.

Season	Start day – End day
Pre-monsoon	1 February – 12 May 2013
Monsoon	13 May – 6 October 2013
Post-monsoon	7 October – 26 October 2013
Winter	27 October 2013 – 31 January 2014

798 **Table 2.** Average values (± standard deviation) of the pollutants, computed for the different seasons
799 selected by the periods of Table 1.
800

	O_3 (nmol/mol)	BC (µg/m^3)	Accum. (#/cm^3)	Coarse (#/cm^3)	PM_1 (µg/m^3)	PM_{10} (µg/m^3)
Pre-monsoon	38.0 ± 25.6	14.5 ± 10.4	668 ± 383	4.2 ± 2.5	98 ± 83	241 ± 134
Monsoon	24.9 ± 16.5	6.3 ± 3.8	250 ± 141	1.9 ± 1.1	32 ± 12	107 ± 37
Post-monsoon	22.8 ± 17.0	6.2 ± 3.9	-	-	26 ± 10	101 ± 38
Winter	20.0 ± 19.8	18.3 ± 14.1	-	-	74 ± 26	320 ± 75
All	27.0 ± 21.3	11.6 ± 10.7	505 ± 372	3.3 ± 2.4	48 ± 42	169 ± 113

801
802

803 **Table 3.** Correlation coefficients (r) between several parameters (BC, O_3, accumulation and coarse
804 particles, WS, T and RAD) for hourly and daily (in parentheses) values, over the whole sampling
805 period.
806

	O_3	BC	Acc.	Coarse	WS	T	RAD
O_3	-	-0.21 (-0.04)	0.11 (0.43)	0.07 (0.41)	0.54 (0.65)	0.51 (0.32)	0.71 (0.56)
BC	-0.21 (-0.04)	-	0.86 (0.78)	0.87 (0.74)	-0.35 (-0.21)	-0.56 (-0.58)	-0.10 (-0.15)
Acc.	0.11 (0.43)	0.86 (0.78)	-	0.86 (0.91)	-0.22 (0.12)	-0.39 (-0.38)	-0.02 (-0.06)
Coarse	0.07 (0.41)	0.87 (0.74)	0.86 (0.91)	-	-0.21 (0.18)	-0.31 (-0.35)	-0.07 (-0.03)
WS	0.54 (0.65)	-0.35 (-0.21)	-0.22 (0.12)	-0.21 (0.18)	-	0.45 (0.41)	0.40 (0.56)
T	0.51 (0.32)	-0.56 (-0.78)	-0.39 (-0.38)	-0.31 (-0.35)	0.45 (0.41)	-	0.43 (0.31)
RAD	0.71 (0.56)	-0.10 (-0.15)	-0.02 (-0.06)	-0.01 (-0.03)	0.40 (0.56)	0.43 (0.31)	-

807

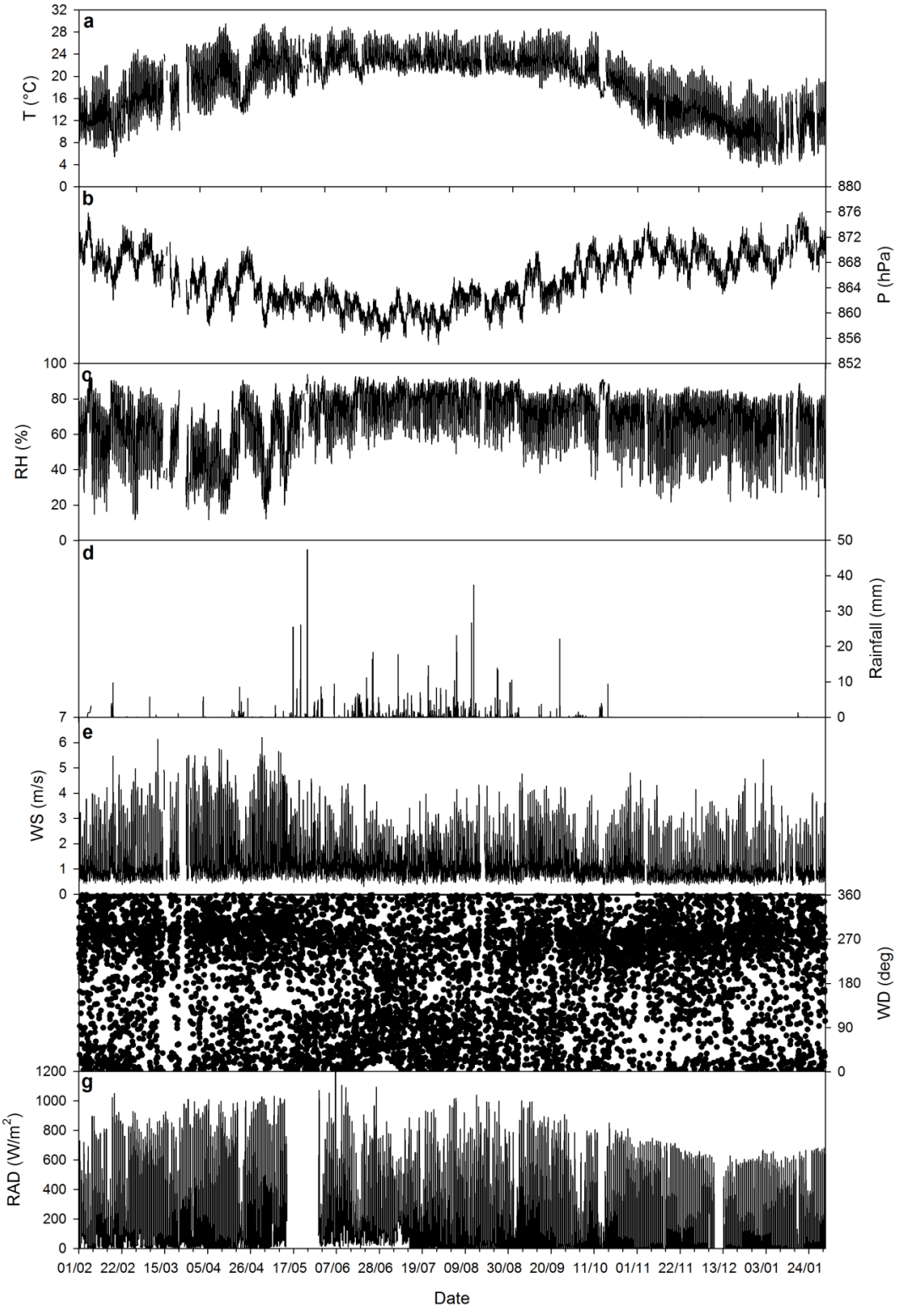

Figure 1. Time series of hourly atmospheric temperature (T, panel *a*), pressure (P, panel *b*), relative humidity (RH, panel *c*), precipitation (*d*), wind speed (WS, panel *e*), wind direction (WD, panel *f*) and solar radiation (RAD, panel *g*) measured at Paknajol.

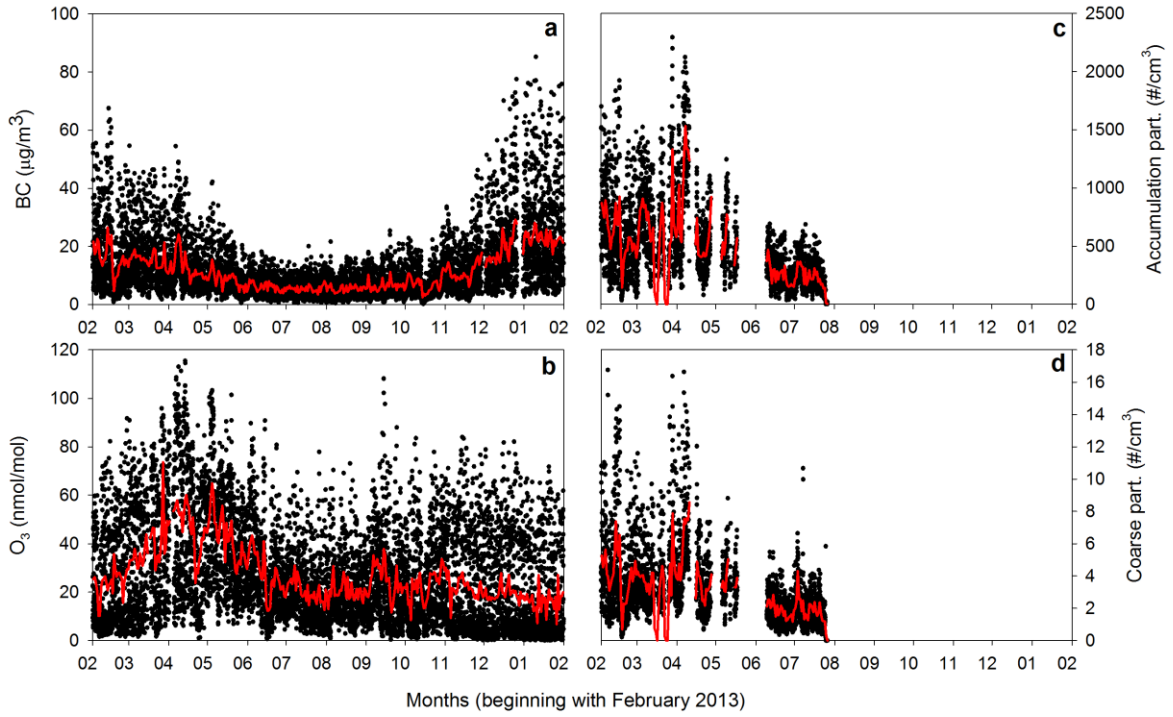

Figure 2. Time series of hourly concentrations of equivalent black carbon (panel *a*), surface ozone (*b*), accumulation (*c*) and coarse particles (*d*) recorded at Paknajol. Red lines denote daily averages.

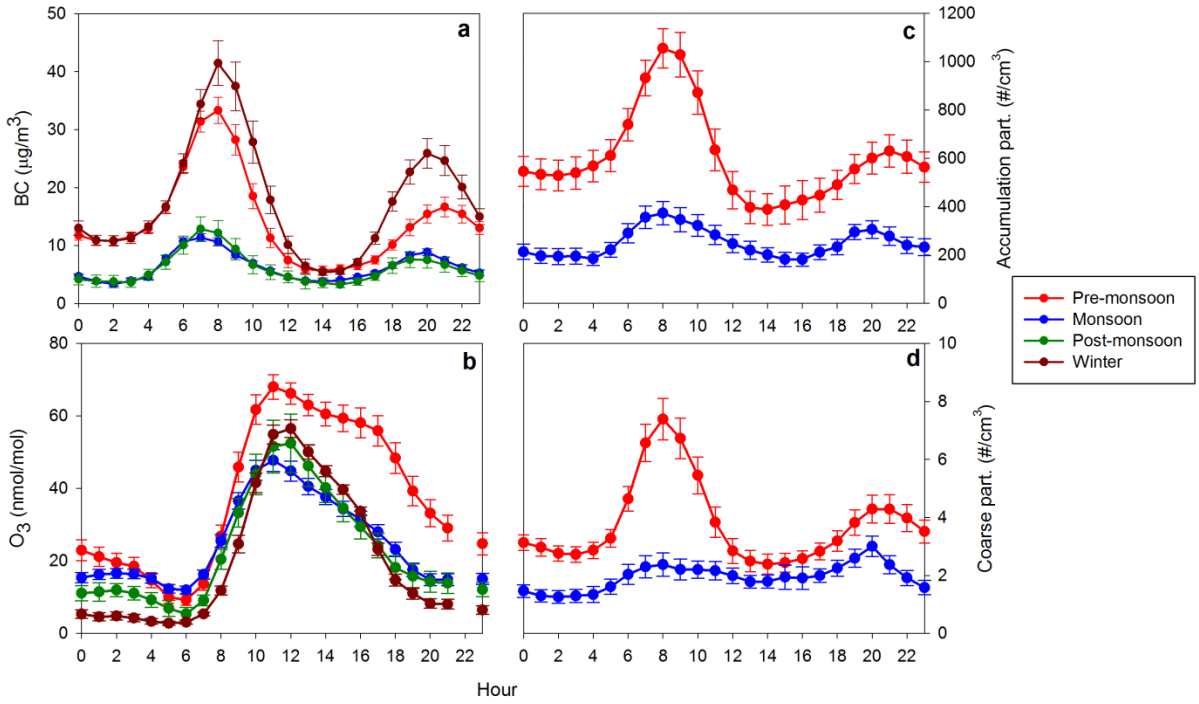

Figure 3. Average seasonal diurnal variation for equivalent black carbon (panel *a*), surface ozone (*b*), accumulation (*c*) and coarse (*d*) particles collected at Paknajol. The error bars denote the expanded uncertainties ($p<0.05$) of the mean.

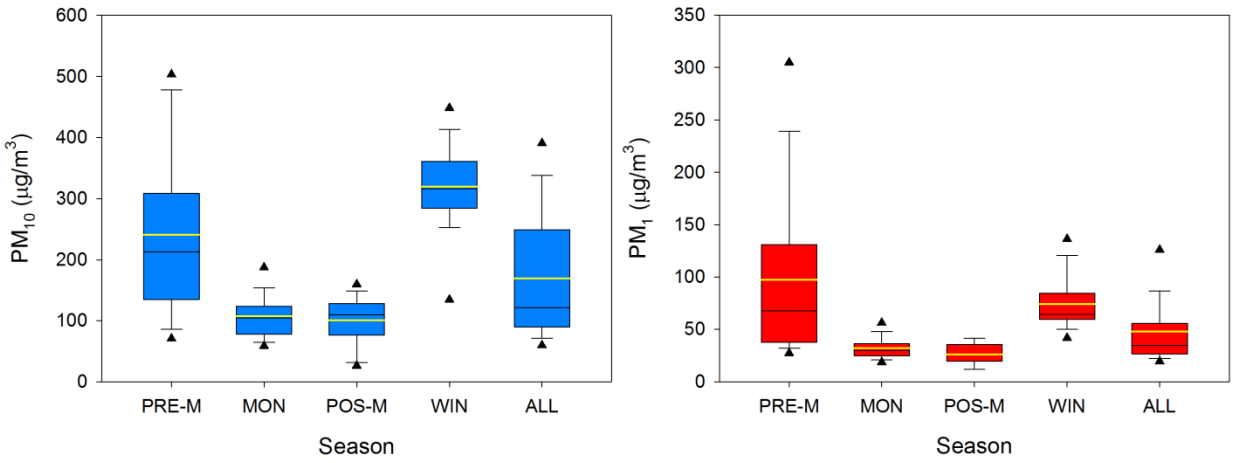

836
837

838 **Figure 4.** Box and whiskers plot for PM_{10} (left panel) and PM_1 (right panel) concentrations at
839 Paknajol, segregated by season (PRE-M: Pre-monsoon, MON: Monsoon, POS-M: Post-monsoon,
840 WIN: Winter and ALL: the whole measurement period). The boxes and whiskers denote the 10^{th},
841 25^{th}, 75^{th} and 90^{th} percentiles of PM values, triangles denote the 5^{th} and 95^{th} percentiles. The median
842 (mean) value is reported as a black (yellow) line.
843
844
845
846
847
848

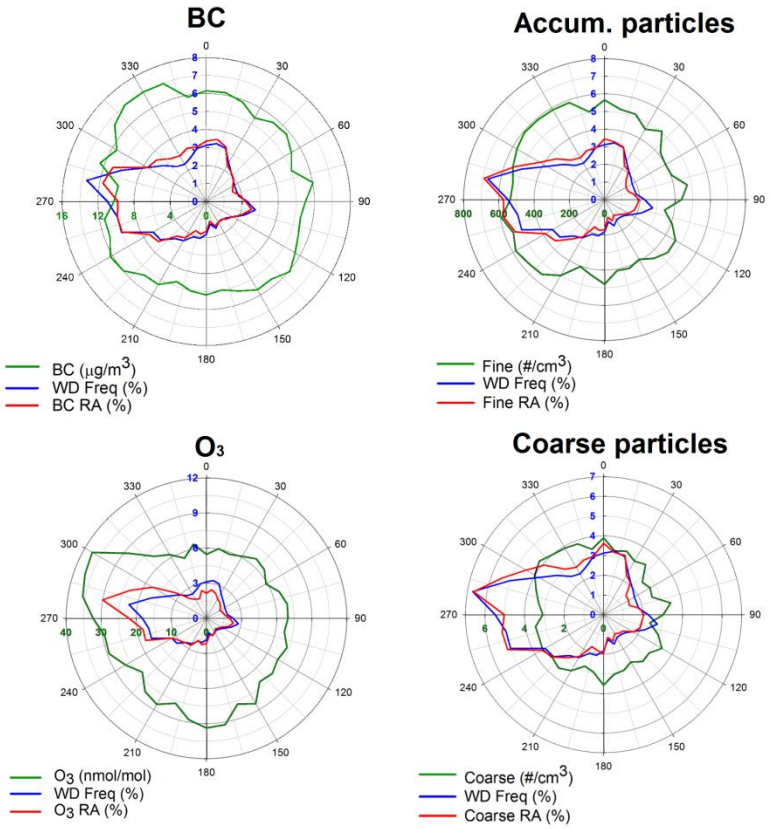

Figure 5. Relation between BC, O_3 (left column), accumulation and coarse particles (right column) and wind direction for Paknajol. The green line represents the mean of respective pollutant per 10° WD interval, the blue line is the relative frequency of WD and the red line is the relative abundance of the chosen pollutant, weighted on the WD frequency, as explained in Gilge et al. (2010).

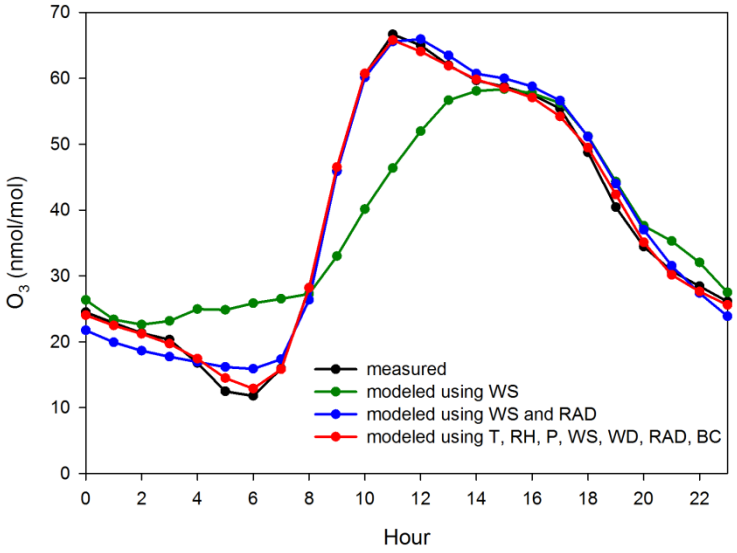

858
859
860 **Figure 6.** Average seasonal diurnal variation of O_3 concentrations for the pre-monsoon period,
861 compared with modelled O_3 using different input parameters (T, RH, P, WS, WD, RAD and BC).
862
863
864
865
866
867
868
869
870
871

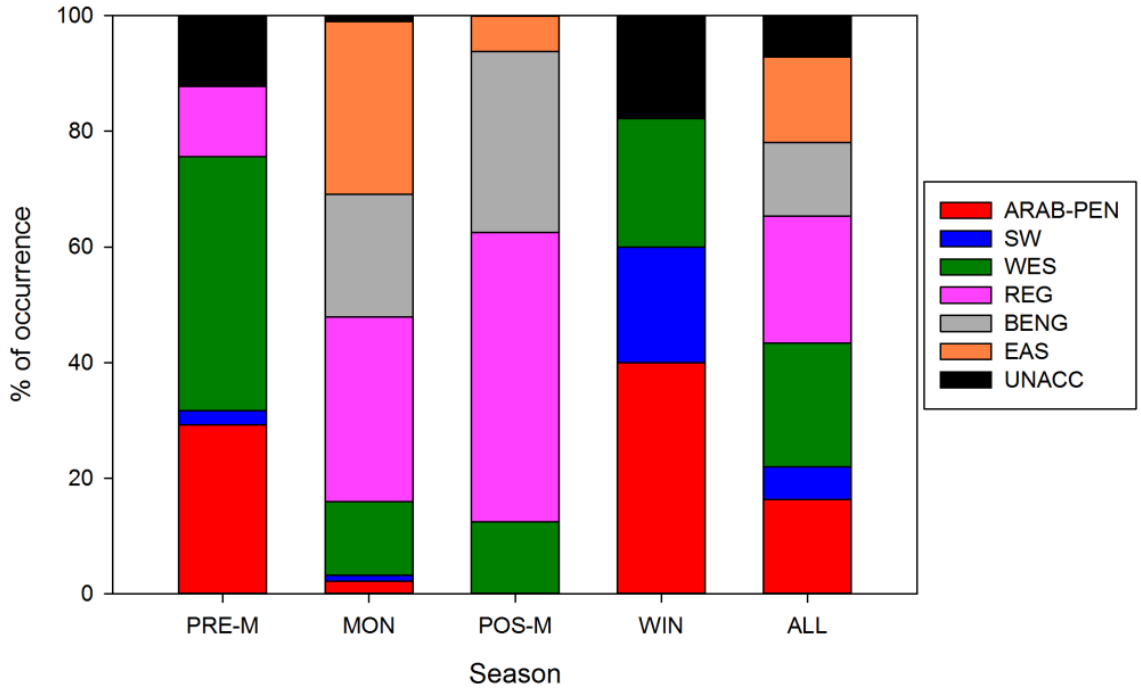

872
873

874 **Figure 7.** Percentage of occurrence registered by the 6 different back-trajectory clusters considered
875 in this work, divided by season (PRE-M: Pre-monsoon, MON: Monsoon, POS-M: Post-monsoon,
876 WIN: Winter and ALL: considering the whole measurement period). Abbreviations for clusters are
877 the following: ARAB-PEN – Arabian Peninsula, SW – South-westerly, WES – Western, REG –
878 Regional, BENG – Bay of Bengal, EAS – Eastern, UNACC – Unaccounted.

879
880
881
882
883
884
885

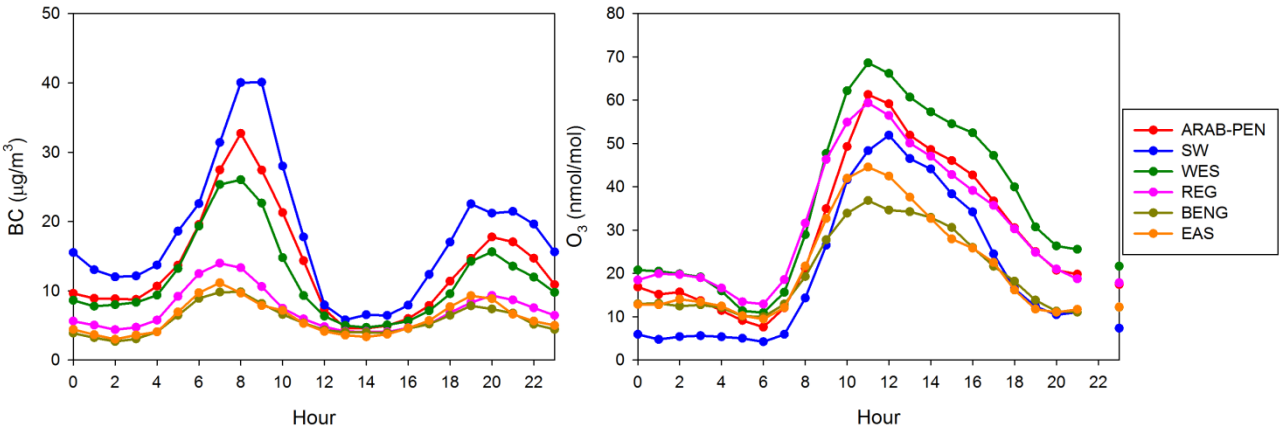

Figure 8. BC (left) and O_3 (right) diurnal variations as a function of the different air-mass clusters shown in Fig. 7. Abbreviations are the following: ARAB-PEN – Arabian Peninsula, SW – South-westerly, WES – Western, REG – Regional, BENG – Bay of Bengal and EAS – Eastern.

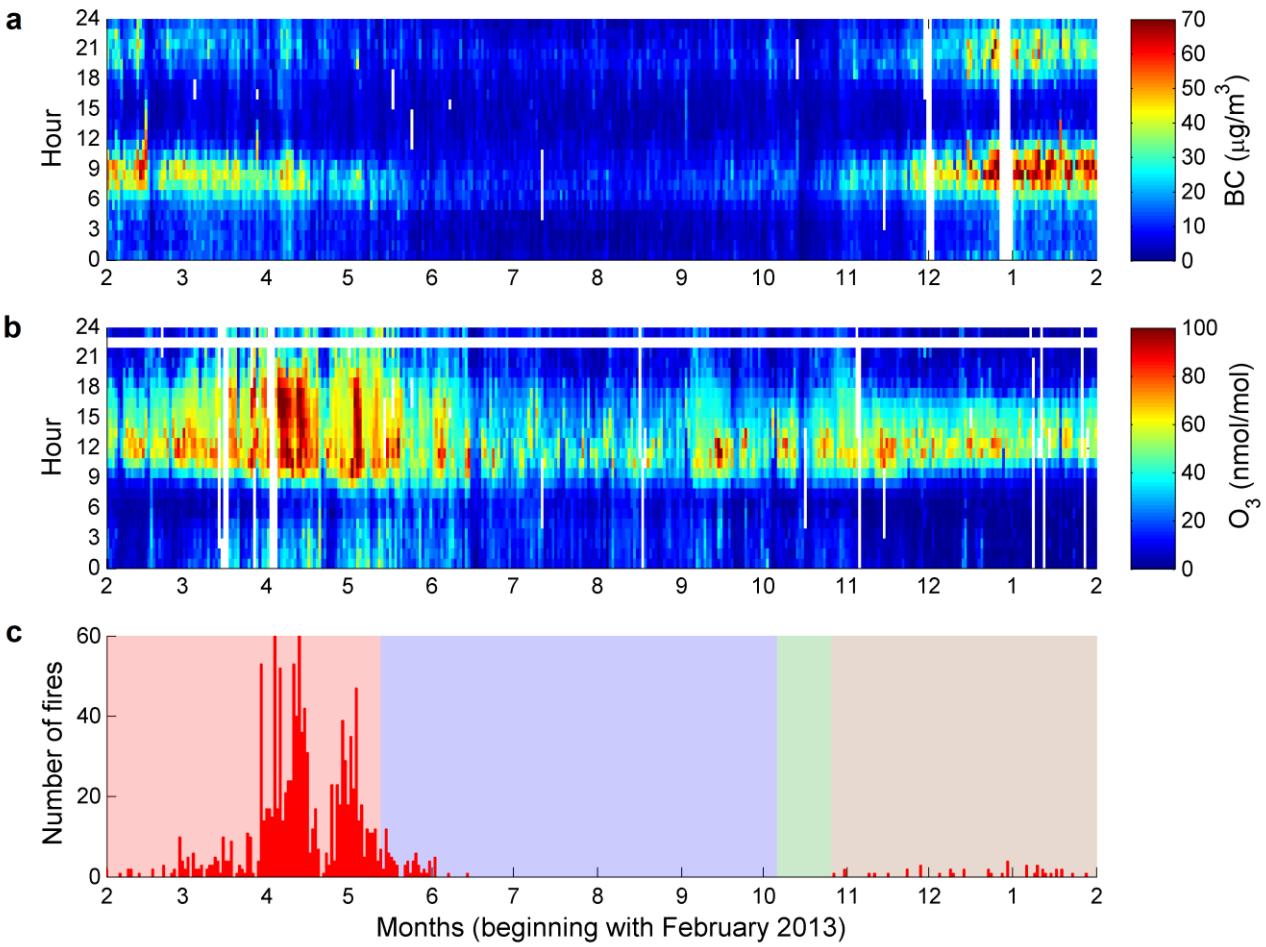

Figure 9. BC (panel *a*) and O_3 (panel *b*) diurnal variations over the entire sampling period. The color scale has been set to a maximum of 70 µg/m^3 and 100 nmol/mol for BC and O_3, respectively. Panel *c* shows the total daily number of fires found in the Southern Himalayas box (see Putero et al., 2014); note that the y-axis has been limited to a maximum value of 60. Shaded areas in panel *c* indicate the different seasons (red: pre-monsoon, blue: monsoon, green: post-monsoon and brown: winter).